

Mechanism of the Stereocomplex Formation between Enantiomeric Poly(lactide)s

Davide Brizzolara* and Hans-Joachim Cantow

Freiburger Materialforschungszentrum FMF and Institut für Makromolekulare Chemie of the University, Stefan-Meier-Str. 21, D-79104 Freiburg, Germany

Kay Diederichs† and Egbert Keller‡

Institut für Biophysik und Strahlenbiologie and Kristallographisches Institut of the University, Freiburg, Germany

Abraham J. Domb

The Hebrew University of Jerusalem, School of Pharmacy, Faculty of Medicine, Jerusalem 91120, Israel

Received August 7, 1995; Revised Manuscript Received October 4, 1995[®]

ABSTRACT: Poly(L-lactide) (PLLA) and poly(D-lactide) (PDLA) crystallize into a stereocomplex with a melting point 50 °C higher than the crystals of the enantiomers. The racemic crystal is formed by packing β -form 3_1 -helices of opposite absolute configuration alternatingly side by side. Single crystals of the stereocomplex exhibit triangular shape. The drastic difference of the powder patterns evidences the different packing of the β -form in the stereocomplex and in crystals of the pure lactides. By force field simulation of the stereocomplex and the PLLA unit cells and of their powder patterns, the reasons for the different packing could be clarified. Between the β -helices in the stereocomplex, van der Waals forces cause a specific energetic interaction-driven packing and, consequently, higher melting point. Helices of identical absolute configuration pack different from pairs of enantiomer β -helices. Packing favors α -type helication. A well-defined 10_2 -helix has not been found. Good agreement with the experimental powder patterns proves the correctness of the simulations. On the basis of morphology, packing calculations, and atomic force microscopy, we propose a model of stereocomplex crystal growth, which explains the triangular shape of single crystals. Thus, for polymer components beyond chain folding length, the stereocomplex formation by simultaneous folding of the two types of chains is plausible. The triangular type of crystallizing offers favorable position for the polymer loops during the crystal growth. Our study of the PLA complexation mechanism may offer a chance to predict other polymeric stereocomplexes and their properties.

Introduction

Poly(L-lactide) (PLLA) has wide applications in medicine because of its biocompatibility and degradability to nontoxic products.¹ Tadokoro showed that poly(*tert*-butylene oxide) and poly(*tert*-butylene sulfide) form racemic lattices, in which *R*- and *S*-chains are arranged side by side in 1/1 proportion.^{2,3} Firstly, it was reported in 1987 that PLLA and poly(D-lactide) (PDLA) crystallize into a 1/1 stereocomplex which exhibits a 50 °C higher melting point than the enantiomeric components.⁴ In the last years many investigations were carried out concerning the physical properties of the stereocomplex. Until now, however, the base for the formation of the complex and its higher stability are unknown.^{4–13} Generally, it was not possible up to now to make a prediction of whether polymers of opposite configuration form stereocomplexes or not. Such predictions are of great interest because of possible applications as biocompatible stereocomplexes.

Thus, the key for understanding special properties is the formation of different helices in the enantiomeric crystals and in the stereocomplex. For example, poly(α -methyl- α -ethyl- β -propiolactone)s of opposite configuration crystallize into a stereocomplex with helical conformation. The components, however, prefer a zig-zag conformation.¹⁴ PLLA and PDLA crystallize to-

gether forming 3_1 -helices. On the other hand the single components do not form a simple 3_1 -helix.^{15–17}

To understand the crystal structure of the components, it is very helpful to clarify the packing of the helices in the stereocomplex, which causes its higher stability. In the following we try to elucidate the stereocomplex and the PLLA arrangement by comparing experimental and simulated data. Furthermore, we calculate the growth rates for the planes of the stereocomplex using symmetry rules to understand complex formation, which competes with the 'homocrystallization' of the enantiomeric crystals.

Experimental Section

Materials. The lactic acids, D(+) and L(-), were purchased from Purac Biochem, Gorinchen, NL. PLLA and PDLA of different molecular weights were synthesized by ring-opening polymerization in toluene with stannous octate as catalyst.^{18,19} The toluene was evaporated out under argon, and the polymer was purified by precipitation in petroleum ether–diethyl ether (1:1, v/v) from a 10% dichloromethane solution. Molecular weights were estimated by gel permeation chromatography in CHCl₃, at a flow rate of 1 mL/min, applying a Spectra Physics (Darmstadt, D) P1000 pump and an Ultrastyrogel column (500 Å pore size, 7.8 × 300 nm size) with UV detection at 254 nm (Applied Bioscience 759A). All data were evaluated with polystyrene standards (Polyscience, Warrington, PA). Further the polymers were characterized by thermal analysis on a Mettler 4000 differential scanning calorimeter. High molecular weight PLLA ($M_n = 333,000$ g mol⁻¹, $M_w = 737,000$ g mol⁻¹) was purchased from Boehringer Ingelheim, D (RS210). The polymers were dried in vacuo and stored in a flask under nitrogen or in an exsiccator over phosphorus pentoxide.

† Institut für Biophysik und Strahlenbiologie.

‡ Kristallographisches Institut of the University.

® Abstract published in *Advance ACS Abstracts*, November 15, 1995.

Powder Diffraction. Powder patterns were measured on a STOE (Darmstadt, D) image plane system at a distance of 130 mm with CuK α radiation. Cell parameters were obtained with local software. PDLA ($M_n = 69,000 \text{ g mol}^{-1}$, $M_w = 128,000 \text{ g mol}^{-1}$) and PLLA RS210 were used to prepare specimens for powder diffraction. Because PLLA and PDLA crystallize analogously, we have taken the powder pattern from PDLA only. We prepared samples from solution as well as from melt. All samples were crushed to small pieces before powder diffraction was applied. Solution crystallization of PDLA was performed as described above. For melt crystallization PDLA was crushed between two glass slides and isothermally crystallized at 155 °C over night. The stereocomplex was crystallized by mixing 3% solutions of PDLA and PLLA in acetonitrile and stirring with 200 r/min at 56 °C. The clear solution became turbid after some hours, and after 2 days, a colorless solid precipitated, the solution again being clear. After 3 days, the solvent was removed with a syringe. The powder pattern of the sample showed only signals of the stereocomplex. The stereocomplex was dried in vacuo for 1 week, to avoid traces of moisture and to prevent solvent from decomposing the polymers when they are heated at elevated temperatures. The stereocomplex was molten at 250 °C and then isothermally crystallized at 180 °C over night.

Atomic Force Microscopy (AFM). A scanning probe microscope (Nanoscope III, Digital Instruments Inc.) was used in this study. Rectangular Si cantilevers (nanoprobes) were applied for the contact mode experiments. Simultaneous registration was performed in the contact mode for height and deflection images. In order to realize good stereocomplex single crystals, relatively low molecular weight partners were applied. The complex was prepared at 56 °C from a 0.1% solution in acetonitrile of PLLA ($M_n = 6,000 \text{ g mol}^{-1}$, $M_w = 16,000 \text{ g mol}^{-1}$) and PDLA ($M_n = 6,000 \text{ g mol}^{-1}$, $M_w = 7,000 \text{ g mol}^{-1}$). Lamellar crystals of PDLA ($M_n = 69,000 \text{ g mol}^{-1}$, $M_w = 128,000 \text{ g mol}^{-1}$) were obtained from a 0.1% solution in acetonitrile at room temperature. The specimens of AFM were prepared by giving 1 drop of the solution on mica and evaporating the solvent by fast spinning.

Molecular Simulation. Exclusively the Cerius² 1.6 version (Molecular Simulations Inc.) was used for the simulations on a Silicon Graphics Indigo² workstation. The polymer chains were built with the Polymer Builder module and packed in the unit cell with the Crystal Builder module. The cell was elongated 3 times in the direction of the *c*-axis to improve the accuracy of the nonbonding interaction calculation along the helix with an Ewald sum.²⁰ In order to simulate an infinitely long helix, the chains were connected in the *c*-direction by bonds between the unit cells. The charges were recalculated during the minimization with the charge equilibrium method.²¹ Packing of the helices was optimized with the Crystal Packer module by minimizing van der Waals and Coulomb energies. Then the atom and cell coordinates were minimized separately with the conjugate gradient 200 algorithm to a root mean square (rms) of 0.05 kcal mol⁻¹ Å⁻¹. The Dreiding 2.21 force field was applied, with modified parameters taken from de Santis and Kovacs for bond lengths, bond angles, and dihedral angles.¹⁵ A Nosé thermostat was used for constant pressure molecular dynamics.

The Diffraction Crystal module was applied for simulation of fiber and powder patterns of the simulated crystal structures. The fiber pattern was simulated with a flat-plate camera type. The peaks in the powder display can be broadened with a Lorentzian profile in order to take into account the crystal size. The full width at half-maximum at angle 2θ is given by the Scherrer equation:

$$\Delta(2\theta)_a = 180 \lambda / (\pi L_a \cos \theta) \text{ etc.} \quad (1)$$

The crystal morphology was calculated with the Bravais–Friedel–Donnay–Harker (BFDH) method. Even if this method is parametrized for small organic molecules and inorganic materials, we have evaluated the morphology of polymer crystals on this basis. The growth rate for a given plane is

calculated with a relation to the inverse plane spacing

$$D \propto 1/d \quad (2)$$

where D is the center-to-face distance and d is the lattice–plane spacing. This relationship explains the growth rate of a given Miller plane in the $hk0$ plane of polymer crystal. In Cerius² the crystal is displayed, and the growth faces can be edited or deleted in a constructed list, thus allowing to build the crystal with the correct faces. The method does not take into account the energetics of the system.

Results and Discussion

Powder Diffraction. Polymer single crystals become only a few micrometers large and, of one folding layer, ca. 10 nm thick. Therefore, with electron diffraction methods only, the *a*- and *b*-axes can be determined. Lamellar crystals of PLLA from *p*-xylyl have an orthorhombic ($a = 1.037 \text{ nm}$, $b = 0.598 \text{ nm}$) or hexagonal ($a = b = 0.590 \text{ nm}$) space group.^{8,22} The *c*-axis and the helix type can be deduced from wide angle X-ray scattering (WAXS) of oriented fibers and films. Until now it was suggested that the pure poly(lactide)s form predominantly an α -type 10₃-helix, even if the observed diffraction patterns exhibit additional reflections which do not fit to a pure 10₃-helix.^{8,15–17} The calculated cell dimensions are pseudoorthorhombic, $a = 1.060 \text{ nm}$, $b = 0.610 \text{ nm}$, $c = 0.288 \text{ nm}$. By variation of the spinning conditions the β -form can be obtained (orthorhombic, $a = 1.031 \text{ nm}$, $b = 1.821 \text{ nm}$, $c = 0.900 \text{ nm}$).¹⁷ Annealing, however, causes irreversible transformation into the α -form.¹⁷ The published results demonstrate significant influence of solvent and specimen preparation on the helix type and the unit cell dimensions.

We tried to make evident the helix type in the solid phase by calculating the cell dimensions from powder diffraction data. The packing of the 3₁-helix and the effective structure of the α -form in PLLA crystals are still unknown. Surprisingly, the powder patterns for solution and melt-crystallized PDLA are identical. From the powder data of Figure 1A, we calculated a unit cell with the *c*-axis that would fit a 10₃-helix. The *a*- and *b*-axes (orthorhombic, $a = 0.710 \text{ nm}$, $b = 0.940 \text{ nm}$, $c = 2.986 \text{ nm}$), however, differ strongly from all cell dimensions published until now. Other calculated cell axes (orthorhombic, $a = 1.000 \text{ nm}$, $b = 0.598 \text{ nm}$, $c = 2.134 \text{ nm}$) also do not explain the reported cell dimensions deduced from X-ray diagrams of oriented fibers. A possible interpretation is an overlapping of α - and β -forms. Taking into account the peaks between 10° and 25° in 2θ exclusively, an orthorhombic unit cell ($a = 1.060 \text{ nm}$, $b = 0.605 \text{ nm}$, $c = 0.940 \text{ nm}$) may be concluded, which fits a 3₁-helix (β -form).

The complex of PLLA and PDLA crystallizes in the β -form exclusively (triclinic, $a = 0.916 \text{ nm}$, $b = 0.916 \text{ nm}$, $c = 0.870 \text{ nm}$, $\alpha = 109.2^\circ$, $\beta = 109.2^\circ$, $\gamma = 109.8^\circ$).⁸ PDLA ($M_n = 69,000 \text{ g mol}^{-1}$, $M_w = 128,000 \text{ g mol}^{-1}$) and PLLA ($M_n = 333,000 \text{ g mol}^{-1}$, $M_w = 737,000 \text{ g mol}^{-1}$) were crystallized into the stereocomplex as described in the Experimental Section. After crystallization from solution, it was recrystallized in the melt at 180 °C. The peaks in the powder pattern of the melt-crystallized stereocomplex (Figure 2B) are more intense than for the solution-crystallized complex (Figure 2A). Thus, the once formed complex is still stable in the melt. The different powder patterns of stereocomplex and PDLA prove the different packing compared with the enantiomer helices.

Force Field Simulation. Because of the poor quality and small size of polymer crystals, it is crucial to

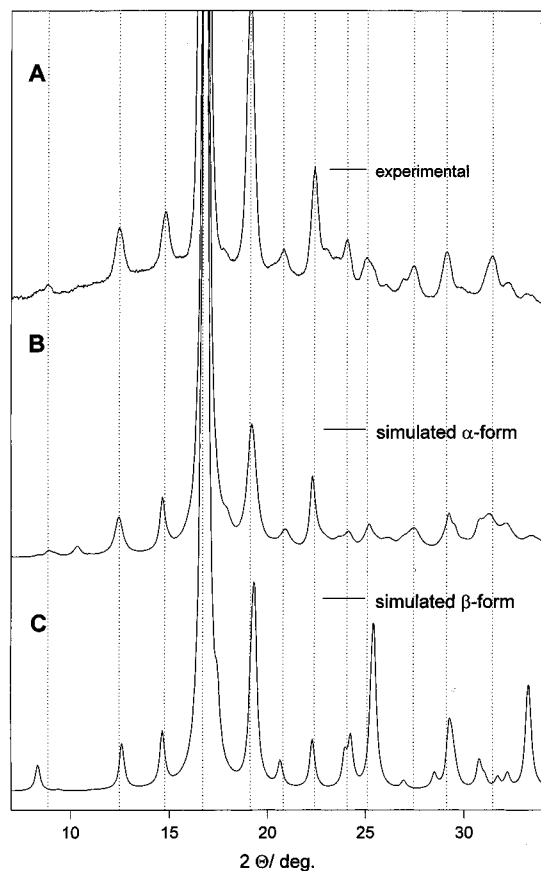


Figure 1. Experimental powder pattern of PLLA (A) and simulated powder patterns of calculated α -PLLA (B) and β -PLLA (C).

Table 1. Simulated 2θ Values of β -PDLA with the Orthorhombic Cell ($a = 1.060$ nm, $b = 0.605$ nm, $c = 0.940$ nm)

hkl	$2\theta_{\text{calcd}}$, deg (I_{rel})
100	8.341 (3.6)
101	12.586 (5.4)
010	14.641 (6.6)
200	16.727 (58.2)
110	16.873 (100.0)
201	19.224 (11.9)
111	19.352 (19.4)
204	20.672 (3.4)
102	22.299 (6.4)
210	22.299 (7.1)
012	23.975 (3.9)
211	24.250 (5.9)
202	25.327 (8.23)
112	25.425 (15.3)
301	26.975 (3.1)
003	28.485 (1.8)
310	29.270 (6.4)
212	29.377 (3.8)
020	29.528 (1.7)
120	30.736 (2.0)
311	30.809 (1.8)
122	32.212 (1.8)
203	33.214 (4.7)
113	33.291 (9.8)

verify the correct position of atoms in the unit cell by X-ray diffraction. Thus, a well-parametrized force field offers a powerful completion to experimental powder data in order to deduce the correct conformation and packing of polymers in the crystalline state. The simulation of diffraction patterns of calculated structures allows direct comparison with experimental results.

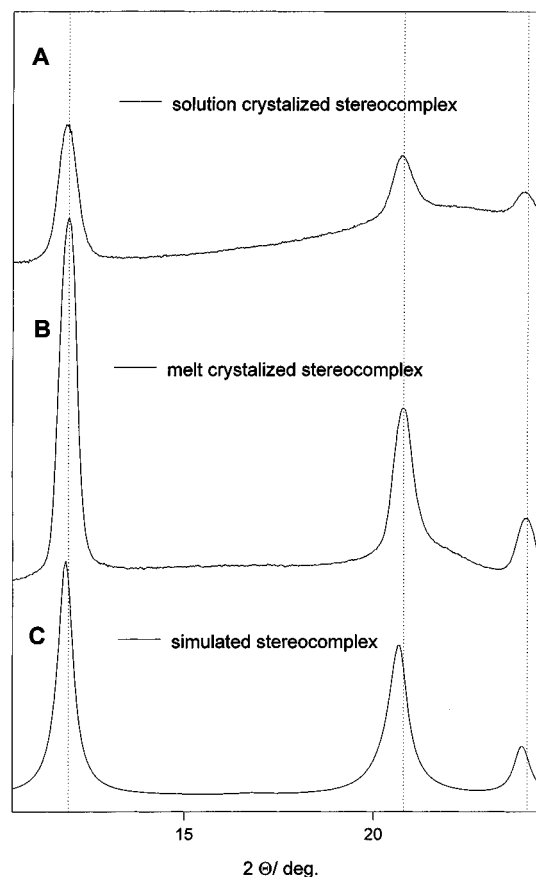


Figure 2. Experimental powder pattern of solution (A) and melt-crystallized (B) stereocomplexes and the simulated powder pattern of the calculated stereocomplex (C).

The minimized structure of the stereocomplex agrees well with the experimental cell dimensions (parallel oriented helices, triclinic $P1$, $a = 0.912$ nm, $b = 0.913$ nm, $c = 0.930$ nm, $\alpha = 110^\circ$, $\beta = 110^\circ$, $\gamma = 109^\circ$; antiparallel oriented helices, triclinic $P\bar{1}$, $a = 0.930$ nm, $b = 0.940$ nm, $c = 0.930$ nm, $\alpha = 111^\circ$, $\beta = 112^\circ$, $\gamma = 108^\circ$). However, the cell dimensions of parallel-oriented helices are closer to the experimental values. The simulated structural models of both orientations in Figure 3 show the same packing of the helices as presented by Okihara et al.⁸ The 3_1 -helix has no mirror plane perpendicular to the chain axis. Thus two non-identical chain orientations are possible. The stereocomplex is formed by two independent helices which may be oriented parallel and antiparallel to each other.⁸ This may also be true for individual enantiomeric chains of higher molecular weight. Adjacent reentry of one chain, however, has the necessary consequence of alternating orientation. The cell parameters of both orientations are quite identical in the stereocomplex, even if the symmetry of the parallel orientation is $P1$ and antiparallel orientation is $P\bar{1}$. In our calculations we applied the arithmetic average of both orientations. With 1.21 g mL⁻¹, the density of the calculated cell is close to the experimental value, 1.24 g mL⁻¹.⁸ The strength profiles of the peaks in the simulated and experimental powder patterns are quite identical, thus proving the correctness of the calculated structure. The PLLA and PDLA helices are arranged in another way. Consequently, stabilizing van der Waals interactions are formed between opposite oxygen atoms and hydrogen atoms. These strong interactions cause the stabilization of the 3_1 -helix and the higher melting point of the complex.

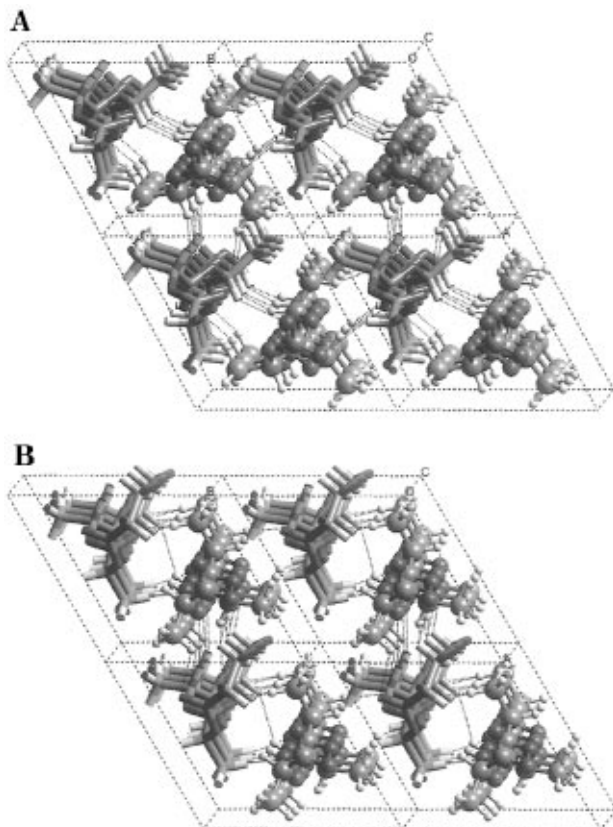


Figure 3. Simulated crystal structure of the stereocomplex (- - -, van der Waals contacts) with parallel orientation of the helices (A) and antiparallel orientation of the helices (B).

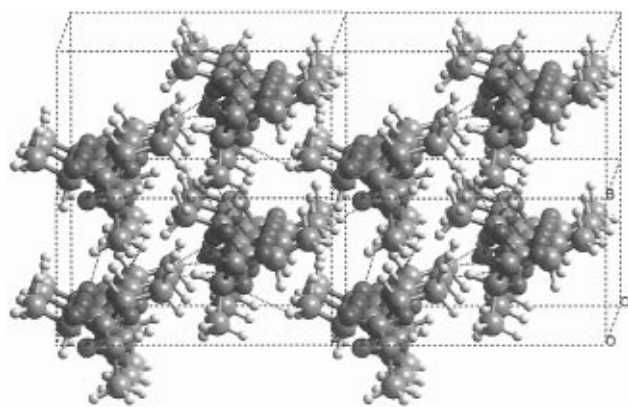


Figure 4. Simulated crystal structure of β -PLLA (- - -, van der Waals contacts).

Figure 4 shows the simulated β -form helices of PLLA, which are arranged to their neighbors in a different way than in the stereocomplex. Thus, such strongly stabilizing interactions are not formed. The different lateral arrangement of the helices, however, achieves a slightly closer packing of the helices than in the complex. The calculated density for the unit cell of β -formed PLLA is 1.26 g mL^{-1} , close to the experimental density of 1.290 g mL^{-1} reported by Pennings.¹⁶ The a - and b -axes of the calculated cell parameters of the orthorhombic cell, $a = 1.058 \text{ nm}$ and $b = 0.576 \text{ nm}$, are close to those experimentally found for lamellar crystals.²² The value of c was found to be 0.935 nm . Using the cell parameters deduced from experimental powder data, the profiles of experimental and simulated powder patterns of Figure 1 are very similar in the angular range from $2\theta = 10^\circ$ to 25° (Table 1). The effective helix must have a similar structure like 3_1 .

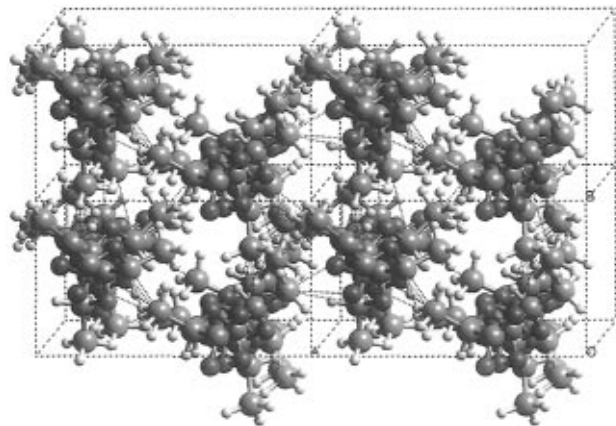


Figure 5. Simulated crystal structure of α -PLLA (- - -, van der Waals contacts).

We tried to understand better the packing of the 3_1 -helix in PLLA by simulating the unit cell where the 3_1 -helices are packed in the same way as in the complex. The minimized structure exhibits other cell parameters (triclinic, $a = 1.220 \text{ nm}$, $b = 0.920 \text{ nm}$, $c = 0.930 \text{ nm}$, $\alpha = 98^\circ$, $\beta = 132^\circ$, $\gamma = 109^\circ$) as the complex. The density of the unit cell of 1.13 g mL^{-1} is smaller than for the other arrangement of the β -helices. This demonstrates the big influence of the absolute helix configuration on packing. Thus, the different orientation of the helices and the stability of the stereocomplex and the pure component crystal essentially are a consequence of interaction caused by the type of packing.

Using periodic boundary conditions, we have calculated the interaction energy (E_{int}) between the helices in the unit cell. For this purpose we calculated first the total energy of the unit cell containing both helices, $E_{(\text{h}_1+\text{h}_2)}$, and then the total energy of the unit cell that contains only one helix, E_{h_1} and E_{h_2} , respectively. The energy difference is the interaction energy between the helices

$$E_{\text{int}} = E_{(\text{h}_1+\text{h}_2)} - (E_{\text{h}_1} + E_{\text{h}_2}) \quad (3)$$

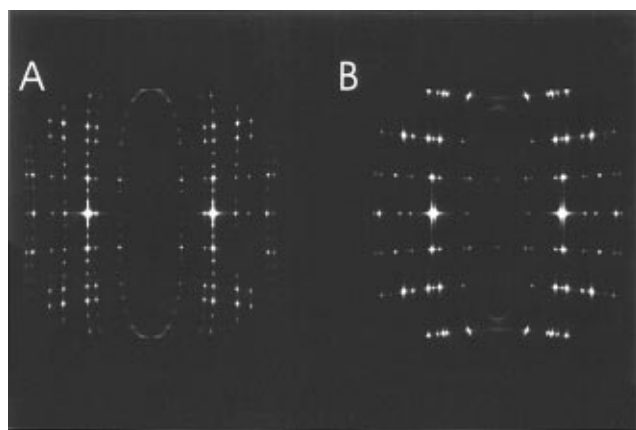
The E_{int} for parallel-oriented ($-119 \text{ kcal mol}^{-1}$) and antiparallel-oriented ($-111 \text{ kcal mol}^{-1}$) stereocomplexes is bigger than that for the enantiomeric crystals ($-91 \text{ kcal mol}^{-1}$). The interaction energy of PLLA with the unrealistic packing of the 3_1 -helix in the stereocomplex manner is smaller ($-96 \text{ kcal mol}^{-1}$) than that for the stereocomplex and not much bigger than that for the correct packing of the β -form helices.

When minimizing the α -form 10_3 -helix usually assumed for PLLA, a distorted 10_3 -helix results, which is less stable than the calculated packing in the β -form. The cell parameters of the distorted 10_3 -helix differ strongly from experimental cell parameters, $a = 1.170 \text{ nm}$, $b = 0.610 \text{ nm}$, $c = 3.140 \text{ nm}$, $\alpha = 90^\circ$, $\beta = 90^\circ$, $\gamma = 97^\circ$. We also tried to pack the 10_3 -helix into the unit cell with the Crystal Packer module as well as by manual shifting in the a - b plane. Simulated and experimental powder patterns do not agree at all.

Constant pressure molecular dynamics starting from the minimized β -form 3_1 -helix show no transformation into the 10_3 -helix after 100 ps. A regular distortion along the chain axis is observed, however, with a 10 monomeric unit periodicity. Taking into account this observation, we propose a PLLA helix which is somewhat distorted from a 3_1 -helix. The sense of distortion—

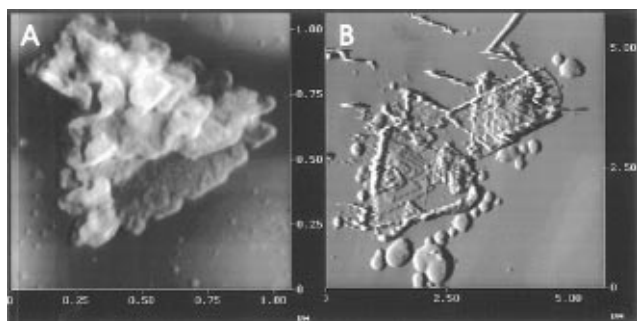
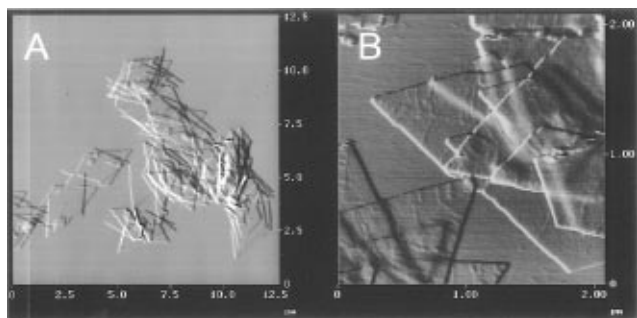
Table 2. Observed and Calculated 2θ Values for Melt-Crystallized α -PDLA with the Orthorhombic Cell ($a = 1.060$ nm, $b = 0.605$ nm, $c = 2.880$ nm)

<i>hkl</i>	2θ , deg (I_{rel})	
	obsd	calcd
100	8.875 (0.6)	8.889 (0.8)
103	12.425 (5.4)	12.440 (5.6)
010	14.775 (6.0)	14.641 (5.1)
104		14.874 (0.6)
011		14.962 (0.4)
200	16.700 (100.0)	16.727 (52.5)
110		16.873 (100.0)
203	19.120 (16.0)	19.128 (11.0)
014		19.257 (17.5)
204	20.800 (1.2)	20.811 (1.3)
114		20.930 (3.5)
015	22.400 (5.7)	22.299 (5.6)
213	24.075 (1.4)	24.172 (2.7)
116	25.100 (1.2)	25.129 (3.3)
300		25.204 (1.3)
207	27.475 (1.6)	27.444 (2.6)
117		27.536 (4.1)
216	29.120 (2.2)	29.118 (3.6)
217		31.241 (5.8)
306	31.475 (2.0)	31.438 (2.4)

**Figure 6.** Simulated fiber pattern of α -PLLA (A) and β -PLLA (B).

left or right—is effected by a slight modification of dihedral angles and is assumed to alternate—in average—after 10 monomeric units. Figure 5 shows such a modified α -form in an orthorhombic unit cell with dimensions $a = 1.060$ nm, $b = 0.605$ nm, and $c = 2.880$ nm. Here, only one dihedral angle was altered for simplicity. It easily succeeds to position the helices in the unit cell in a way that experimental and simulated powder patterns agree very well (Figure 1B and Table 2). The simulated fiber patterns for the β - and α -forms of Figure 6 agree well with experimental patterns published from DeSantis and Pennings.^{15–17} We are not able to minimize the proposed α -form of PLLA to a rms smaller than 1 kcal mol⁻¹ Å⁻¹. This seems not to be crucial, however, because the simulated diffraction patterns support the correctness of the proposed structure more conclusively than an energetic calculation. We suggest that the instability of the pure 3₁-helix is caused by the packing and that it leads to the distortion along the chain axis, without transformation into a 10₃-helix. We propose to call the discussed helix model a distorted 3₁-helix α -form. Rietveld calculations may offer an ultimate decision concerning its arrangement.

Morphology. Lamellar stereocomplex crystals exhibit an uncommon triangular shape (Figure 7). The single-component crystals have a lozenge (Figure 8) or hexagonal form. The PLLA and PDLA chains pack

**Figure 7.** AFM images of stereocomplex single crystals.**Figure 8.** AFM images of PDLA single crystals.**Table 3. Calculated Growth Faces of the Lamellar Stereocomplex**

<i>hkl</i>	center-to-face distance (<i>D</i> , nm)	lattice—plane spacing (<i>d</i> , nm)	area of growth faces (nm ³)	corners
001	0.43870	2.25292	77.09846	6
00 $\bar{1}$	0.43870	2.25292	77.09846	6
010	1.34114	0.74564	16.89307	4
0 $\bar{1}$ 0	1.34114	0.74564	16.89370	4
100	1.34274	0.74475	16.83355	4
$\bar{1}$ 00	1.34274	0.74475	16.83355	4
1 $\bar{1}$ 0	1.34911	0.74123	16.59400	4
$\bar{1}$ 10	1.34911	0.74123	16.59400	4
110	2.32015	0.43101		
$\bar{1}$ $\bar{1}$ 0	2.32015	0.43101		
1 $\bar{2}$ 0	2.33120	0.42896		
$\bar{1}$ 20	2.33120	0.42896		
2 $\bar{1}$ 0	2.33398	0.42845		
$\bar{2}$ 10	2.33398	0.42845		

different in their enantiomeric crystals than in the stereocomplex, with the consequence of differing morphologies. The growth rate of the possible growth faces was calculated in relation to the inverse spacing. The respective sides of crystals are formed predominately by low-order Miller planes. The observation is explained by the fact that thin slices (high-order faces) attach to each other better than thick slices (low-order faces). Thus, we suggest that the BFDH method calculates the correct growth rate for a given Miller plane in the $hk0$ plane of a polymeric lamellar crystal. The BFDH method yields a hexagonal crystal (Table 3) because the opposite Miller planes have identical probability to grow. The racemic stereocomplex, however, does not form a hexagonally shaped crystal. Growing in opposite directions forms triangular crystals which look similar, having opposite Miller planes, however. With an edit/delete list of the growth faces, we have constructed the corresponding crystal morphology.

The growth direction of the side of a crystal is parallel, though fast growing faces or Miller planes become small but the faces or Miller planes perpendicular to them become large. The (110), (1 $\bar{2}$ 0), and (2 $\bar{1}$ 0) Miller planes are perpendicular to the ($\bar{1}$ 10), (100), and (0 $\bar{1}$ 0) Miller planes; consequently, the respective sides of the trian-

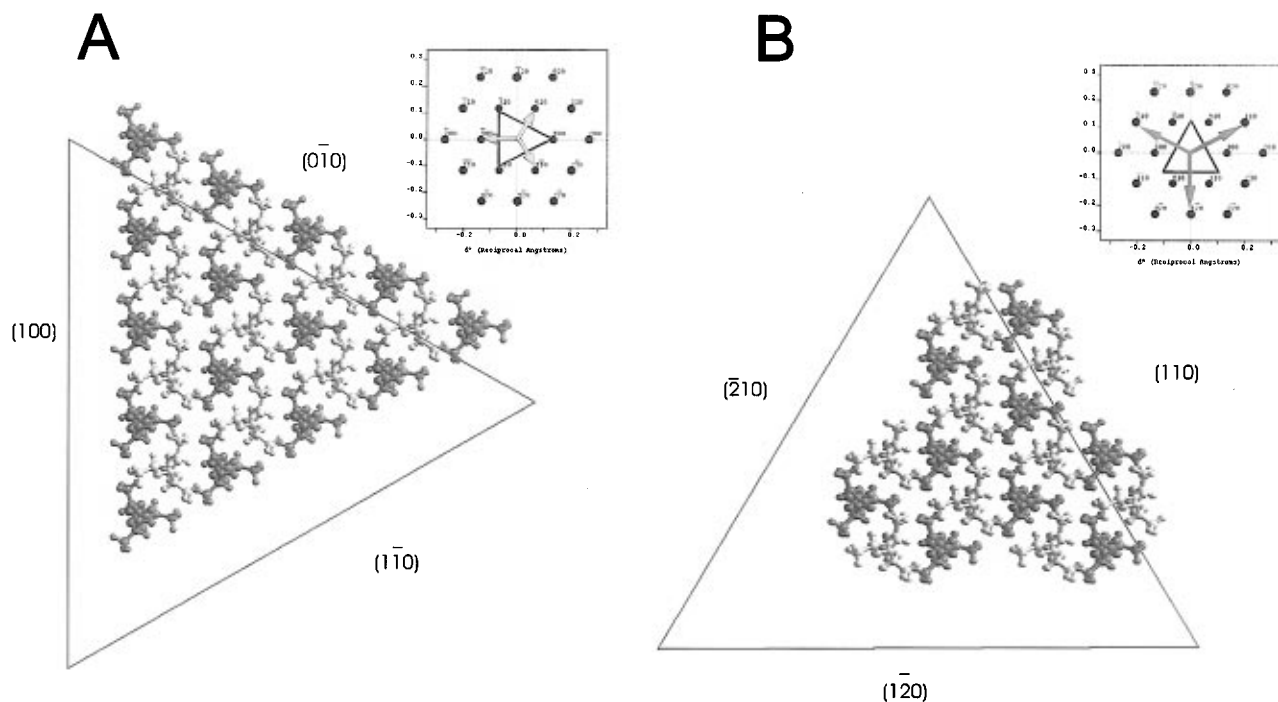


Figure 9. Simulated morphology and helix packing of the stereocomplex single crystal: (A) calculated morphology and (B) morphology proposed from Okihara et al.

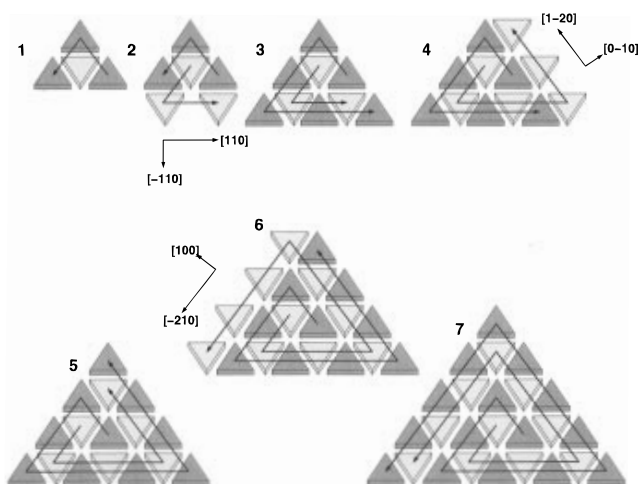


Figure 10. Schematic growing mechanism of the stereocomplex single crystal.

gular stereocomplex crystal can be formed from one set of these Miller planes. The calculated growth rates for the (110) , $(1\bar{2}0)$, and $(\bar{2}10)$ Miller planes are bigger than those for the $(\bar{1}10)$, (100) , and $(0\bar{1}0)$ planes. Consequently, the $(\bar{1}10)$, (100) , and $(0\bar{1}0)$ Miller planes are the respective sides of the stereocomplex single crystal. Packing of the helices along these Miller planes forms the triangular crystal of Figure 9A. It is unlikely that the (110) , $(\bar{2}10)$, and $(1\bar{2}0)$ planes are the respective sides of the stereocomplex single crystal. Figure 9B shows the growth tendency of such a crystal. The fastly growing (110) , $(\bar{2}10)$, and $(1\bar{2}0)$ Miller planes are more rough, however, than the (100) , $(0\bar{1}0)$, and $(\bar{1}10)$ planes.

Okihara et al. have indicated the (110) , $(\bar{2}10)$, and $(1\bar{2}0)$ Miller planes for the respective sides of the stereocomplex single crystal from a transmission electron microscopic image and the diffraction pattern.⁸ A mistake might occur identifying the Miller planes of the respective faces. In our model of Figure 9A, the respective sides of the stereocomplex are formed by PLLA or

PDLA exclusively. Which poly(lactide) actually forms the surface depends on its position in the unit cell.

Taking into account the morphology and packing of the PDLA and PLLA helices in the stereocomplex, we have illustrated in Figure 10 a possible growing mechanism for the triangular lamellar crystal. We suggest that in the beginning of the crystallization, for example, PDLA will be surrounded by PLLA. Caused by the triangular shape of the 3_1 -helix, a triangular nucleus is formed whose respective sides are built up exclusively by PLLA. In the next step a PDLA layer grows on the crystal surface. Then again a PLLA layer grows onto the PDLA layer and so on. Our model agrees well with the calculated growth faces. Furthermore, the alternating growth of PDLA and PLLA layers offers a favorable position of the independent loops for both types of enantiomeric macromolecules. In addition, the 60° angle of the respective sides to each other avoids overcrossing of the PLLA and PDLA loops during crystallization.

Conclusions

On the basis of molecular simulation, we propose a model that explains the stability and formation of the poly(lactide) stereocomplex. The complexation of PDLA and PLLA leads to a stabilization of the helices which causes an increased stability. Because the force field is sensitive to sterical effects, we hope to predict similar effects for other stereocomplexes. The proposed growing mechanism for the stereocomplex single crystal may also explain the complex formation in the melt.

A distorted α -form, 3_1 -helix is proposed for the enantiomeric crystals, on the basis of molecular simulations and experimental data. Further simulations including molecular dynamics as well as investigations on the crystallization behavior of the single poly(lactide)s will be done to refine the structure of the distorted 3_1 -helix.

References and Notes

- (1) Kronenthal, R. L., Oser, Z., Martin, E., Eds. *Polymer Science and Technology, Polymers in Medicine and Surgery*; Plenum

- Press: New York, 1975; Vol. 8.
- (2) Sakakihari, H.; Takahashi, Y.; Tadokoro, H.; Oguni, N.; Tani, H. *Macromolecules* **1973**, *6*, 205.
 - (3) Matsubayashi, H.; Chatani, Y.; Tadokoro, H.; Dumas, P.; Spassky, N.; Sigwalt, P. *Macromolecules* **1977**, *10*, 996.
 - (4) Ikada, Y.; Jmshidi, K.; Tsuji, H.; Hyon, S.-H. *Macromolecules* **1987**, *20*, 906.
 - (5) Tsuji, H.; Horii, F.; Hyon, S.-H.; Ikada, Y. *Macromolecules* **1991**, *24*, 2719.
 - (6) Tsuji, H.; Hyon, S.-H.; Ikada, Y. *Macromolecules* **1991**, *24*, 5651.
 - (7) Tsuji, H.; Hyon, S.-H.; Ikada, Y. *Macromolecules* **1991**, *24*, 5657.
 - (8) Okihara, T.; Tsuji, M.; Kawaguchi, A. Katayama, K.-I.; Tsuji, H.; Hyon, S.-H.; Ikada, Y. *J. Macromol. Sci. Phys.* **1991**, *B30* (1 and 2), 119.
 - (9) Tsuji, H.; Hyon, S.-H.; Ikada, Y. *Macromolecules* **1992**, *25*, 2940.
 - (10) Tsuji, H.; Ikada, Y. *Macromolecules* **1992**, *25*, 5719.
 - (11) Tsuji, H.; Horii, F.; Nakagawa, M.; Ikada, Y.; Odani, H.; Kitamaru, R. *Macromolecules* **1992**, *25*, 4114.

- (12) Tsuji, H.; Ikada, Y.; Hyon, S.-H.; Kimura, Y.; Kitao, T. *J. Appl. Polym. Sci.* **1994**, *51*, 337.
- (13) Tsuji, H.; Ikada, Y. *J. Appl. Polym. Sci.* **1994**, *53* (8), 1061.
- (14) Prud'homme, R. E.; Ritcey, A. M. *Makromol. Symp.* **1993**, *73*, 203.
- (15) De Santis, P.; Kovacs, A. J. *Biopolymers* **1968**, *6*, 299.
- (16) Eling, B.; Gogolewski, S.; Pennings, A. J. *Polymer* **1982**, *23*, 1578.
- (17) Hoogsteen, W.; Postema, A. R.; Pennings, A. J.; Brinke, G. ten; Zugenmaier, P. *Macromolecules* **1990**, *23*, 634.
- (18) Kulkarni, R. K.; Moore, E. G.; Heygyelli, A. F.; Leonard, F. *J. Biomed. Matter Res.* **1971**, *5*, 109.
- (19) Dittrich, V. W.; Schulz, R. C. *Angew. Makromol. Chem.* **1971**, *5*, 169.
- (20) Karasawa, N.; Goddard, W. A., III. *J. Phys. Chem.* **1989**, *93*, 7320.
- (21) Rappé, A. K.; Goddard, W. A. *J. Phys. Chem.* **1991**, *95*, 3358.
- (22) Kalb, B.; Pennings, A. J. *Polymer* **1980**, *21*, 607.

MA951144E